

Methanol Electrooxidation Reaction in Alkaline Medium on Glassy Carbon Electrode Modified with Ordered Mesoporous Ni/Al₂O₃

Yan Wang, Wei Chen, Dahai Pan, Qian Xu, Jinghong Ma, Jiajun Zheng, Ruifeng Li*

College of Chemistry and chemical Engineering, Taiyuan University of Technology, Taiyuan, 030024, People's Republic of China

*E-mail: rfli@tyut.edu.cn

Received: 17 November 2016 / Accepted: 18 January 2017 / Published: 12 February 2017

In this work, ordered mesoporous Ni/Al₂O₃ catalysts were prepared by the solvent evaporation induced self-assembly (EISA) method. The synthesized Ni/Al₂O₃ catalysts were characterized by XRD, elemental distribution analyses, N₂ adsorption and TEM. Ni/Al₂O₃ modified glassy carbon electrode was used to investigate the electrocatalytic oxidation of methanol in 0.1 M NaOH solution by cyclic voltammetry (CV) and chronoamperometry (CA). CVs results showed good electrocatalytic activity of Ni/Al₂O₃ for methanol electrooxidation in alkaline electrolytes. The good methanol electrooxidation activity of Ni/Al₂O₃ could be attributed to its synergetic effects between high dispersion of nickel and the ordered mesoporous structure that facilitates the diffusion of methanol and products. The CV and CA results suggest methanol electrooxidation is an irreversible process and a diffusion controlled process. The rate constant for the catalytic reaction of methanol is calculated to be $1.66 \times 10^6 \text{ cm}^3 \text{ mol}^{-1} \text{ s}^{-1}$.

Keywords: Methanol Electrooxidation, Glassy Carbon Electrode, Direct Methanol Fuel Cell, Alkaline Medium

1. INTRODUCTION

Direct methanol fuel cell (DMFCs) is considered to be a promising power source for transportation, portable electronics and other applications due to its high energy conversion efficiency, low pollution emission and simple operation [1–3]. However, there are several technical problems hindering the commercialization of DMFCs, which include the methanol permeability from the anode to the cathode [4] and the relatively slow kinetics of methanol oxidation reaction (MOR) on the anode [5]. Using alkaline electrolyte can be a feasible approach for the development of DMFCs due to the

electrocatalytic oxidation of methanol in alkaline medium is kinetically faster than in acidic medium [6, 7]. Moreover, the usage of alkaline electrolytes in DMFCs presents other advantages such as less sensitive to poisoning effects [8, 9] and lower corrosion. The electrode materials play an important role in the electrocatalytic oxidation of methanol. Pt-based materials such as Pt and PtRu are commonly used as anode catalyst for MOR. However, the high cost and rareness of Pt largely restrict the broad commercialization of DMFCs. In alkaline electrolytes, a much wider range of low cost materials can be used as anode catalysts such as Zn, Ni, Pd and other non-noble transition metals. Among these materials, nickel is a promising catalytic material due to its surface oxidation properties [10].

Porous materials such as zeolite are widely used as the supports for electrocatalysis reaction. The high surface area and large pore volume of the supports are critical in electrocatalysis due to the high surface area and large pore volume can allow better dispersion of metal catalysts and facilitate the diffusion of reactants and products [11]. Recently, nickel supported porous materials have been employed for methanol electrooxidation and exhibit good electrocatalytic activity [12, 13].

In this work, nickel supported ordered mesoporous alumina were prepared by the solvent evaporation induced self-assembly (EISA) method. Then, the electrocatalytic oxidation of methanol on ordered mesoporous Ni/Al₂O₃ modified glassy carbon electrode in alkaline solution have been studied by the methods of cyclic voltammetry and chronoamperometry.

2. EXPERIMENTAL

2.1 Preparation and characterization of ordered mesoporous Ni/Al₂O₃

Ni/Al₂O₃ catalysts were synthesized by the solvent evaporation induced self-assembly (EISA) method. The typical synthesis procedure is described as follows: 3.2 g triblock copolymer F127 ($M_w=126,000$, Sigma-Aldrich) was fully dissolved in 20 mL absolute ethanol containing 1.6 g hydrochloric acid (37 wt.%) and 0.4 g citric acid. 3.26 g aluminum isopropoxide and a certain amount of nickel nitrate (2.32, 0.93 and 0.47 g, respectively) were added into the above solution slowly. The mixture was stirred vigorously at 32 °C for 24 h. Then, the obtained solution was transferred into a dish and further underwent solvent evaporation at 45 °C for 48 h and 100 °C for 24 h, respectively. The Ni/Al₂O₃ catalysts were obtained by calcination of the products at 400 °C for 5 h with 1 °C/min after evaporation. The Ni/Al₂O₃ catalysts were named as Ni/Al₂O₃- x , where x indicates the molar ratio of Al/Ni.

X-ray powder diffraction (XRD) patterns were recorded on a SHIMADZU XRD-6000 diffractometer with Cu K α radiation. Langmuir and Brumauer-Emmett-Teller (BET) surface areas, pore volume and pore size distribution of the samples were determined by analyzing N₂ adsorption/desorption isotherms on a Quantachrome NOVA 1200 instrument at 77 K. Elemental distribution analysis of the catalysts were conducted by using a HITACHI S-4800 scanning electron microscope equipped with energy dispersive spectroscopy (EDS). Transmission electron microscopy (TEM) images were obtained on a JEOL JEM-2100 microscope operated at 200 kV. The samples

were well dispersed in ethanol by sonication. Then, a carbon coated Cu TEM grid was dipped into the sample suspension and dried under vacuum at 80 °C.

2.2 Electrochemical measurement

Cyclic voltammetry (CV) and chronoamperometry studies were carried out by using a CHI electrochemical workstation (model 600B, Shanghai, China). A home-made one-compartment three-electrode cell was employed with Ag/AgCl as the reference electrode (3M KCl), Pt wire as the counter electrode and Ni/Al₂O₃ modified glassy carbon electrode (GCE, geometric area is 0.0707 cm²) as the working electrode. All the electrochemical tests are conducted at room temperature.

Before modification, the glassy carbon electrode were polished to a mirror-like surface with alumina slurry on a polishing cloth, then rinsed with deionized water (DI water) and ultrasonicated in DI water and absolute ethanol for 10 minutes, respectively. The Ni/Al₂O₃ modified GCEs were prepared as follows: 10 mg of Ni/Al₂O₃, 5 mg carbon black were dispersed ultrasonically in 5 μL of 5 wt.% Nafion solution, 0.2 mL isopropanol and 0.795 mL of DI water to form a suspension. Then, 5 μL of this suspension was pipetted directly on the polished surface of GCE and dried in air at room temperature for 4 h to obtain the Ni/Al₂O₃ modified GC. For comparisons, Pt (20%)/C and carbon black modified GCE were also fabricated in the same way.

3. RESULTS and DISCUSSION

3.1 Characterization of Ni/Al₂O₃

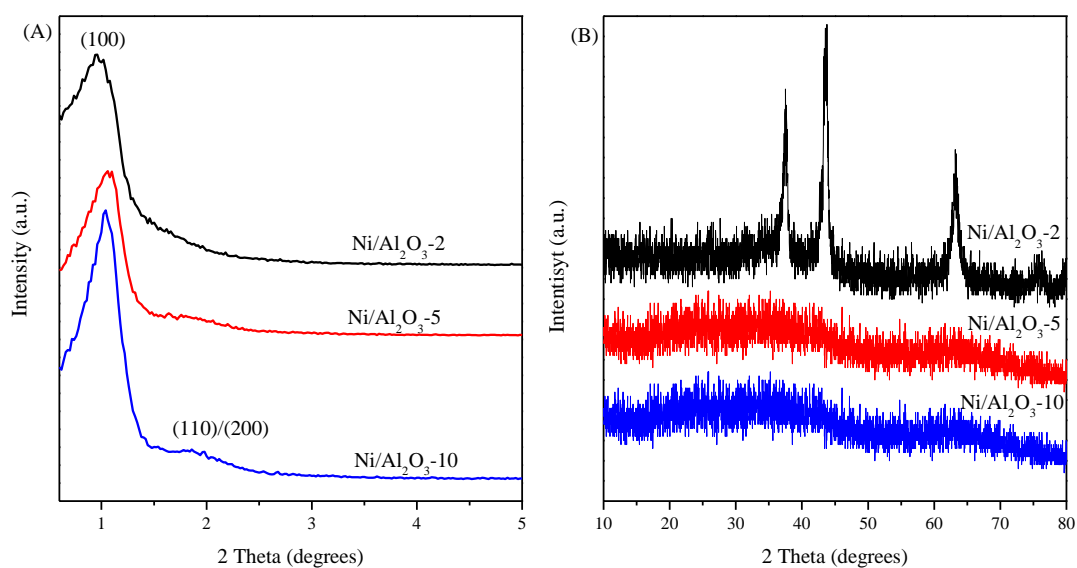


Figure 1. Low (A) and wide (B) angle XRD patterns of Ni/Al₂O₃ catalysts with different Al/Ni molar ratios.

XRD measurements were performed to investigate the crystalline structure of the Ni/Al₂O₃ catalysts. In figure 1A, a strong diffraction peak at 1.0° and a broad peak at ~1.9° on Ni/Al₂O₃-10 could be observed, which are characteristics of (100) and (110)/(200) planes in catalysts with highly ordered mesoporous structure [14]. Diffraction peaks at 1.0° and broad peak at ~1.9° could still be observed on Ni/Al₂O₃-2 and Ni/Al₂O₃-5, but the intensity of the diffraction peaks decreases along with the Ni content increasing which indicates the regular mesoporosity decreasing. Figures 1B shows the wide angle XRD patterns of Ni/Al₂O₃ catalysts. Ni/Al₂O₃-2 exhibits the characteristic diffraction peaks of crystalline NiO phase (JCPDS #: 47-1049) at 37.6°, 43.7°, 63.1° and 75.8°. Due to the relatively high content of nickel in Ni/Al₂O₃-2, a portion of nickel existed in the mesoporous channels of Al₂O₃ in the form of nickel oxide nanoparticles. No diffraction peaks of NiO could be observed on Ni/Al₂O₃-5 and Ni/Al₂O₃-10, which suggests the highly dispersion of nickel on these two catalysts. In other words, the nickel species had been homogeneously incorporated into the mesoporous matrix of Al₂O₃ in Ni/Al₂O₃ catalysts.

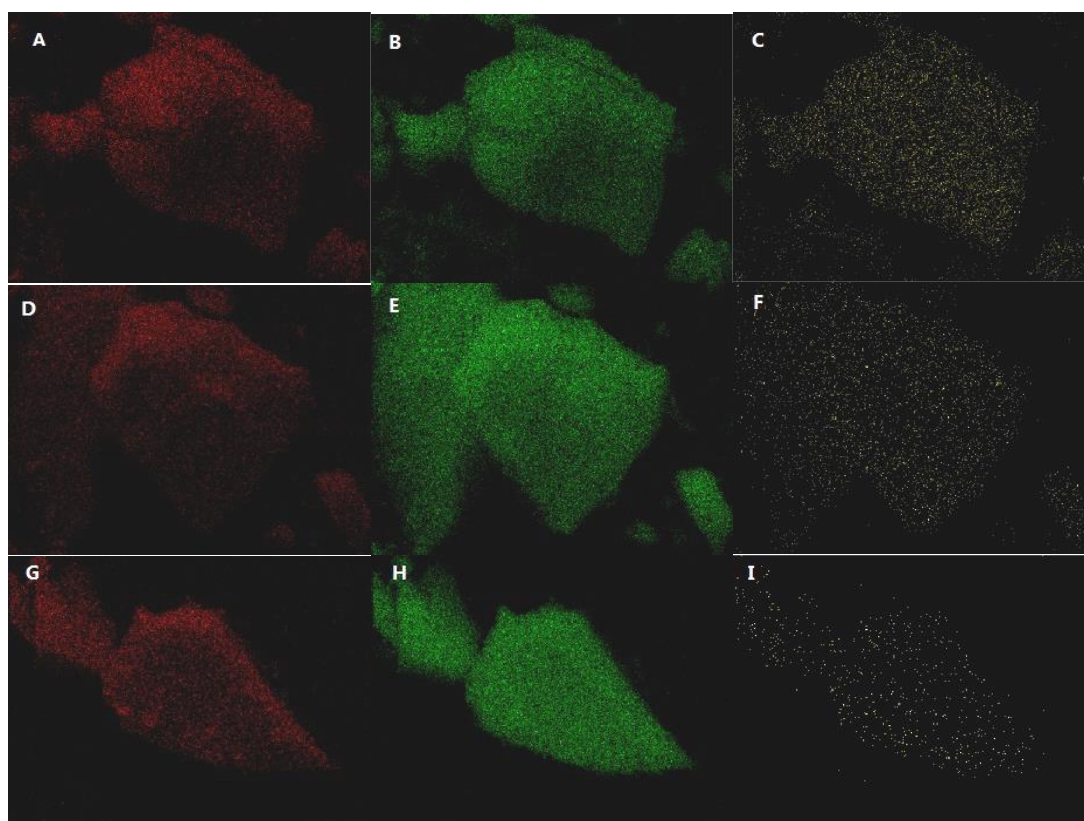


Figure 2. Elemental mapping analyses of Ni/Al₂O₃-2 (A, B, C), Ni/Al₂O₃-5 (D, E, F) and Ni/Al₂O₃-10 (G, H, I) showing the distributions of O (red), Al (green) and Ni (yellow).

Elemental mapping analyses of Ni/Al₂O₃ are shown in Figure 2. The elemental mapping images further confirm the highly homogenous distributions of elements O, Al and Ni in the Ni/Al₂O₃ catalysts.

The nitrogen adsorption–desorption isotherms and the corresponding pore distributions of Ni/Al₂O₃ catalysts are shown in Figure 3. In Figure 3A, all of the catalysts exhibit typical IV type isotherms with H1 type hysteresis loops, which further indicates the presence mesoporous structure of the catalysts. Ni/Al₂O₃–5 and Ni/Al₂O₃–10 demonstrate narrow pore size distributions in Figure 2B, indicating ordered mesoporous structure of the catalysts. Compared with Ni/Al₂O₃–5 and Ni/Al₂O₃–10, Ni/Al₂O₃–2 exhibits relatively wide pore size distribution due to partial nickel species exist on the external surface of alumina support. Moreover, the detailed structure properties of Ni/Al₂O₃ obtained from the isotherms are summarized in Table 1. With the nickel content increasing in the catalysts, the BET surface area (S_{BET}) and the pore volume of Ni/Al₂O₃ decrease gradually. Meanwhile, the mesopore diameters of Ni/Al₂O₃ are centered in the range of 6.2 – 7.7 nm.

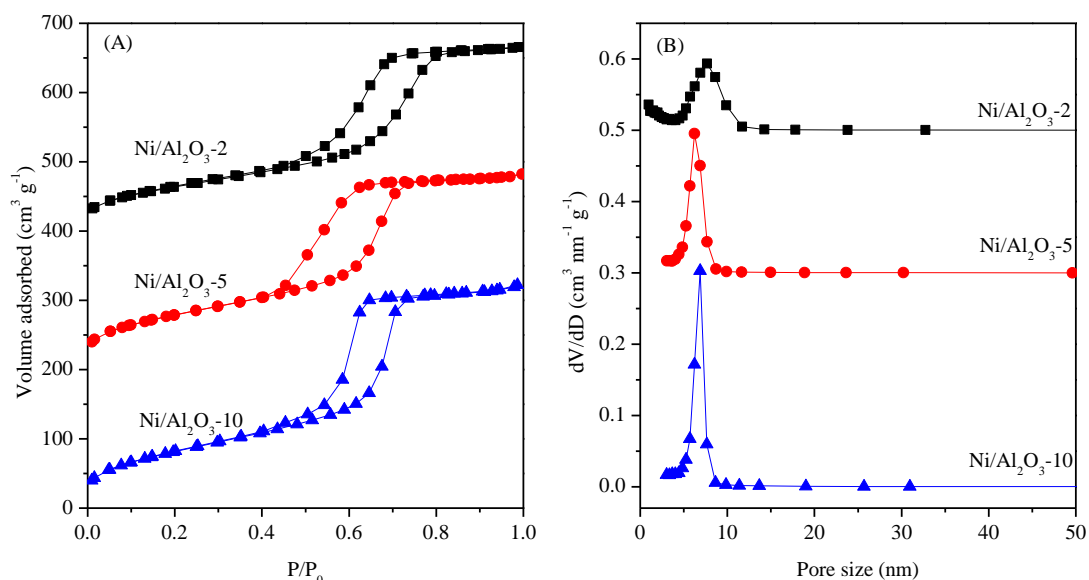


Figure 3. N₂ adsorption–desorption isotherms (A) and the corresponding pore size distributions curves (B) of the Ni/Al₂O₃ catalysts. In (A), the isotherms of Ni/Al₂O₃–2 and Ni/Al₂O₃–5 are offset along the Y axis by 400 and 200 cm³ g^{–1}, respectively. In (B), the pore size distributions of Ni/Al₂O₃–2 and Ni/Al₂O₃–5 are offset by 0.5 and 0.3 cm³ nm^{–1} g^{–1}, respectively.

Table 1. The structural parameters of Ni/Al₂O₃ obtained from N₂ adsorption isotherms analysis.

Catalyst	S_{BET} (m ² /g)	Pore volume (cm ³ /g)	Pore diameter (nm)
Ni/Al ₂ O ₃ –2	237	0.41	7.7
Ni/Al ₂ O ₃ –5	290	0.44	6.2
Ni/Al ₂ O ₃ –10	304	0.50	6.9

It can be observed from the TEM images of Ni/Al₂O₃ (Figure 4), all of the samples exhibit ordered mesoporous channels. And the diameters of mesopore obtained from TEM images are in good agreement with the values calculated from nitrogen adsorption–desorption isotherms, suggesting the

mesoporous structure of Ni/Al₂O₃. Moreover, NiO nanoparticles with the diameter over 100 nm can be observed on Ni/Al₂O₃-2, which is in good agreement with the XRD results.

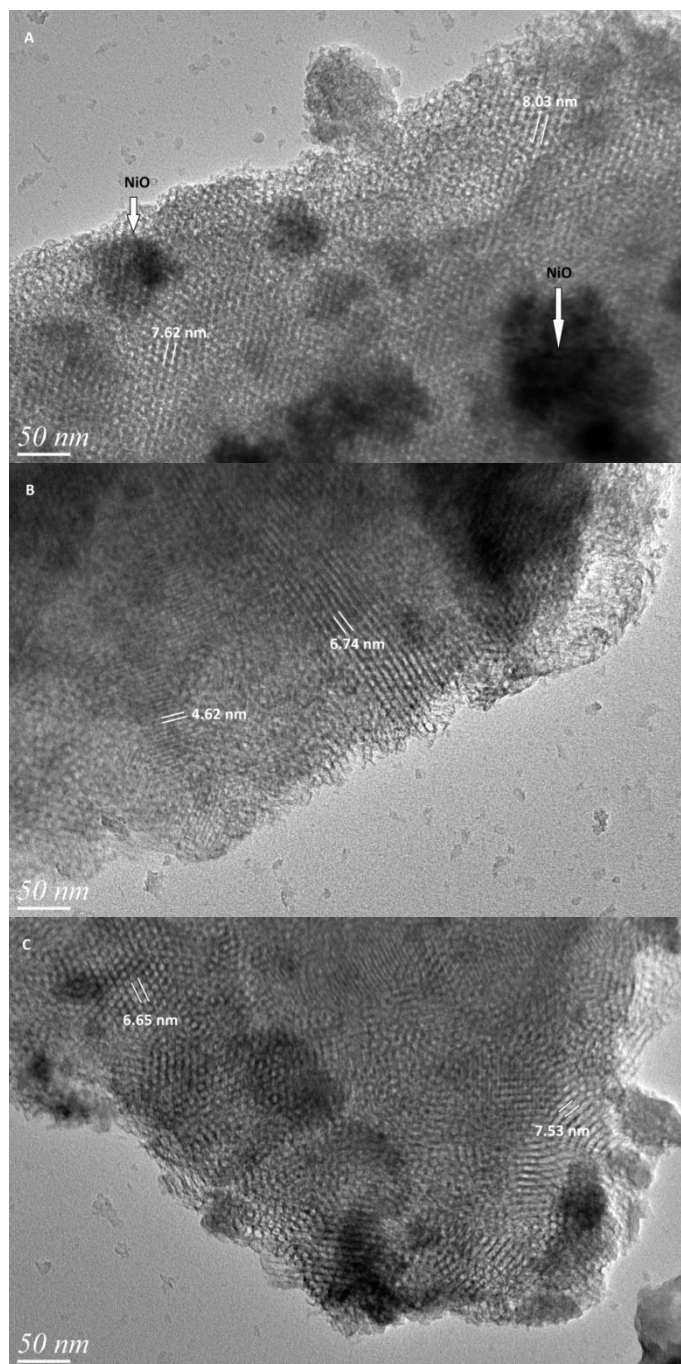


Figure 4. TEM images of Ni/Al₂O₃-2 (A), Ni/Al₂O₃-5 (B) and Ni/Al₂O₃-10 (C).

3.2 Electrochemical behavior of Ni/Al₂O₃

3.2.1 Electrocatalytic oxidation of methanol at Ni/Al₂O₃

Figure 5 shows the cyclic voltammograms of Ni-Al₂O₃-5/GCE in the absence and presence of 0.1 M methanol in 0.1 M NaOH solution. According to the electrochemical behavior of nickel

electrode in alkaline electrolyte, thin layer of Ni(OH)₂ forms spontaneously on nickel surface and nickel is electrochemically passivated by Ni(OH)₂ coating [15, 16]. As can be seen in Figure 5a, a peak in the anodic direction at 0.62 V was observed on CV of Ni/Al₂O₃-5 in the absence of methanol, which represents the oxidation of Ni(OH)₂ to the nickel oxy-hydroxide (NiOOH). Meanwhile, the peak could be observed in the cathodic direction at 0.44 V. This peak can attribute to the reduction of NiOOH to Ni(OH)₂ [17, 18], in accordance with the following reaction [19]:

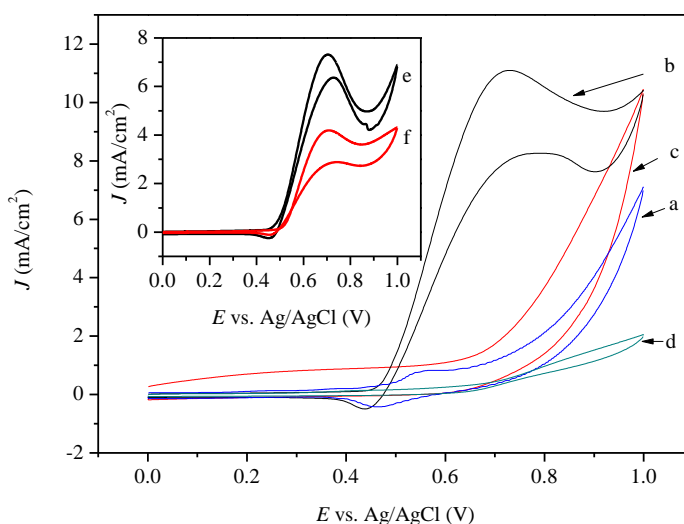
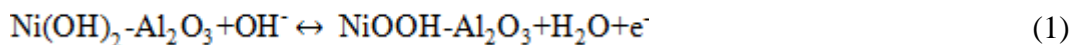
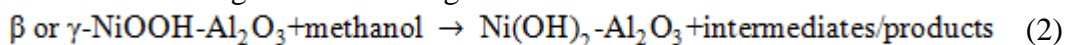


Figure 5. Cyclic voltammograms of Ni/Al₂O₃-5 in the absence (a) and presence of 0.1 M methanol (b) in 0.1 M NaOH at a scan rate of 20 mV/s. Comparison of CVs at Pt/C (c) and carbon black (d) modified GCE in the presence of 0.1 M methanol in 0.1 M NaOH at a scan rate of 20 mV/s. The inset shows the CVs of Ni/Al₂O₃-2 (e) and Ni/Al₂O₃-10 (f) in 0.1 M NaOH with 0.1 M methanol at a scan rate of 20 mV/s.

In comparison CVs of Ni/Al₂O₃-5 in absence and presence of 0.1 M methanol in 0.1 M NaOH (Figure 5a and 5c), considerable anodic current was observed for methanol electrooxidation. The methanol electrooxidation takes place at the onset potential of the NiOOH species starts to be formed, which indicates NiOOH species are the electrocatalytic active species for methanol electrooxidation. At the reverse scan in presence methanol, there is a peak at 0.78 V which is due to the regeneration of active sites for the adsorption methanol at the higher potential value.

The reduction peaks could also be observed in presence of methanol, however, the current value are much smaller than that in absence of methanol. The decrease of the cathodic peak height in presence of methanol is attributed to the partial consumption of NiOOH species for methanol electrooxidation according to the following reaction:



No obvious current peak of methanol oxidation on CV of Pt/C modified GCE could be observed in 0.1 M NaOH and 0.1 M methanol solution (Figure 5b), indicating Pt/C obtains no obvious methanol electrooxidation activity in alkaline medium, which is in accordance with the literature report

[20]. Moreover, there is no clear oxidation peak could be observed on carbon black modified GCE (Figure 5d), which indicates black carbon only works as the electron conducting support.

Table 2. Comparisons of the peak potential (E_p) and the peak current density (J) reported for methanol electrooxidation on various Ni based electrodes.

Electrode	E_p (V)	J (mA/cm ²)	ν (mv/s)	Ref.
Ni-Co/GC	0.63 vs. Ag/AgCl	3.9	20	[21]
Ni(II)OPD/GC ^a	0.57 vs. SCE	9.9	20	[22]
Ni-ZSM-5/CPE ^b	0.72 vs. Ag/AgCl	9.2	20	[23]
Ni-NiY/CPE ^b	0.78 vs. Ag/AgCl	5.5	20	[24]
Ni-SBA-15/CPE	0.80 vs. Ag/AgCl	14.2	25	[25]
Ni-NZM/CPE ^c	0.83 vs. Ag/AgCl	8.3	50	[26]
Ni(OH) ₂ /GC	0.58 vs. Ag/AgCl	15.4	50	[27]
Poly-Ni(II)-curcumin/GC	0.77 vs. Ag/AgCl	14.2	100	[28]
Ni/Al ₂ O ₃ -2/GC	0.70 vs. Ag/AgCl	7.3	20	This work
Ni/Al ₂ O ₃ -5/GC	0.72 vs. Ag/AgCl	11.1	20	This work
Ni/Al ₂ O ₃ -10/GC	0.70 vs. Ag/AgCl	4.2	20	This work

^a OPD, Bis(1,2-phenylenediamine) Nickel (II), ^b CPE, Carbon Paste Electrode, ^c NZM, nano-ZSM-5 zeolite.

Table 2 presents the peak potential and the peak current density on Ni/Al₂O₃/GC electrode toward the methanol electrooxidation. In comparison with other Ni based electrode, this ordered mesoporous structure Ni/Al₂O₃ catalyst could be a competitive candidate for methanol electrooxidation.

The CVs of Ni/Al₂O₃-2 and Ni/Al₂O₃-10 in presence of 0.1 M methanol are shown in Figure 5e and 5f, respectively. These two catalysts with different Ni contents both exhibit clear methanol oxidation peaks at 0.70V. The comparisons of E_p and j with different electrodes for methanol electrooxidation are summarized in Table 2. Among Ni/Al₂O₃ with different Ni contents (Al/Ni=2, 5 and 10), Ni/Al₂O₃-5 exhibited the highest current density. Compared with Ni/Al₂O₃-5, Ni/Al₂O₃-10 shows lower current density due to its lower Ni content in the catalyst. However, the catalyst Ni/Al₂O₃-2 with the highest nickel content did not exhibit the highest activity in the methanol electrooxidation due to the fact that its mesoporous structure and nickel dispersion have been sacrificed. Mesoporous structure and highly dispersion of metals are regarded to be an efficient way to increase the methanol electrooxidation activity [20]. Therefore, the excellent methanol electrooxidation activity of Ni/Al₂O₃-5 can be attributed to synergetic effects between homogeneously dispersed nickel active species and relatively high ordered mesoporosity that improves the diffusion of methanol and reaction products.

3.2.2 Effects of scan rate on the methanol electrooxidation at Ni/Al₂O₃

Figure 6A shows CVs of Ni/Al₂O₃-5 in the presence of 0.1 M methanol in 0.1 M NaOH at different scan rates of 10–300 mV/s. With the scan rates increasing, the peak potentials for methanol

electrooxidation shift to positive potentials, while the cathodic peak potentials for reduction of NiOOH shift to negative potential, indicating a kinetic limitation in methanol oxidation between the redox sites NiOOH/NiOH and methanol.

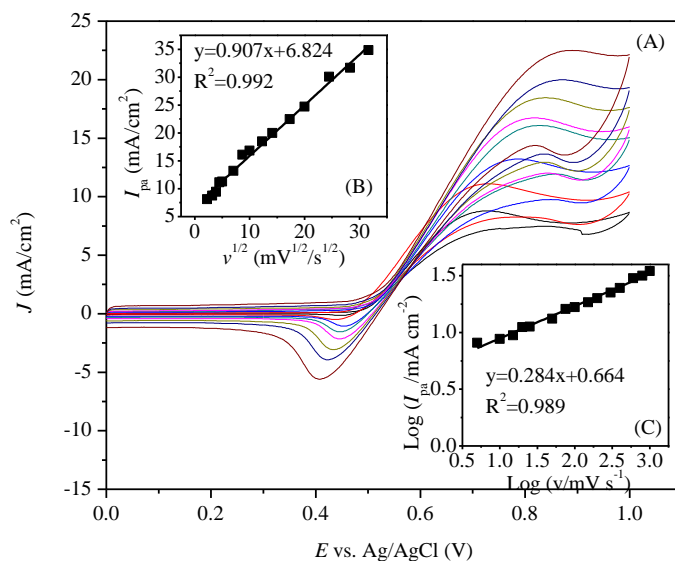


Figure 6. (A) Cyclic voltammograms of Ni/Al₂O₃-5 in 0.1 M NaOH containing 0.1 M methanol at various scan rates (from inner to outer): 10, 20, 50, 75, 100, 150, 200, 300 mV/s. (B) The inset shows the anodic peak current density (I_{pa}) versus the square root of scan rates (5–1000 mV/s). (C) The inset shows plots of $\log I_{pa}$ versus $\log v$.

Figure 6B inset shows a plot of anodic peak current density versus the square root of scan rates from 5 to 1000 mV/s in 0.1 M methanol with 0.1 M NaOH solution. The plot of I_{pa} versus the square root of scan rates shows a linear in the range of scan rates 5–1000 mV/s, indicating the methanol electrooxidation process is diffusion controlled. Thus, diffusion could be a key factor that affects the methanol electrooxidation activity under our experimental conditions. Figure 6C shows the plots of $\log I_{pa}$ versus $\log v$ in the scan rates from 5 to 1000 mV/s, and the slope is calculated to be 0.284. In theory, the slope of $\log I_{pa}$ versus $\log v$ plots is 1.0 or 0.5, which is regarded as the methanol electrooxidation is adsorption controlled or diffusion controlled, respectively [25, 29]. According to literature [30], this low value suggests the charge transfer for methanol oxidation on Ni/Al₂O₃ is relatively slow and the methanol oxidation is controlled by combined diffusion and kinetic limitation.

3.3.3 Effect of methanol concentration

Figure 7A shows the CVs of Ni/Al₂O₃-5 in 0.1 M NaOH with different concentration of methanol. Only the anodic scan curves are showed for the purpose of clarity. With the methanol concentration increasing, the peak potentials of methanol electrooxidation shift to positive potentials and the current densities of methanol electrooxidation increase. Meanwhile, the cathodic peak keeps decreasing along with methanol concentration increasing (Figure 7B inset), suggesting that the rate–

determining step is methanol involved [31]. Figure 7C inset shows the plots of anodic peak current density versus methanol concentration. It can be observed that it is not linear correlation between anodic peak current density and methanol concentration. There are two linear segments with methanol concentration at 0.2 M as the inflection point, indicating that the mechanism and the rate-determining step vary along with methanol concentration increasing. When methanol concentration is below 0.2 M, the methanol oxidation is the rate-determining step. While the methanol concentration is above 0.2 M, the methanol oxidation and removal of adsorbed intermediates turn to be the rate-determining step.

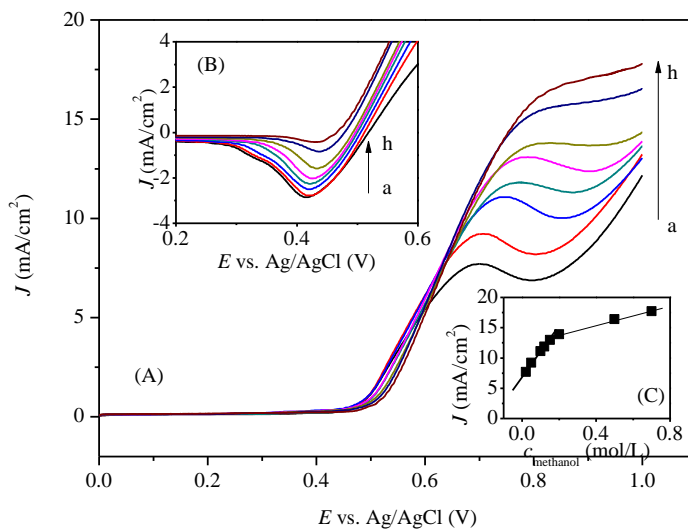


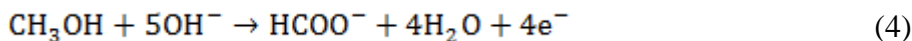
Figure 7. (A) Cyclic voltammograms (only the anodic scan curves are presented) of Ni/Al₂O₃-5 in 0.1 M NaOH in presence of (a) 0.02 M, (b) 0.05 M, (c) 0.1 M, (d) 0.12 M, (e) 0.15 M, (f) 0.2 M, (g) 0.5 M, (h) 0.7 M of methanol at a scan rate of 20 mV/s. (B) Inset shows the zoomed reverse scan CVs of Ni/Al₂O₃ in 0.1 M NaOH containing different methanol concentrations. (C) Inset shows the plots of anodic peak current density versus methanol concentration.

3.3.4 Chronoamperometry studies

Chronoamperometry was employed to measure the catalytic rate constant and the diffusion coefficient of methanol on Ni/Al₂O₃-5 modified GCE. Figure 8 shows the double-step chronoamperograms of Ni/Al₂O₃-5 by setting the applied potentials at 720 mV (in first step) and 300 mV (in second step) at different concentration of methanol. The transient current is due to the methanol oxidation and the current density is negligible when the potential step down to 300 mV, which indicates the methanol electrooxidation is an irreversible process [19]. The net current density I_{net} (obtained by subtracting the background current) is linearly dependent on the inverse of the square root of time $t^{-1/2}$ (Figure 8B). This result suggests that the methanol oxidation is under the dominance of the methanol diffusion. The value of diffusion coefficient of D of methanol is calculated to be $3.4 \times 10^{-6} \text{ cm}^2/\text{s}$ by using the slope of this line in Cottrell equation [19]:

$$I_{\text{net}} = nFAD^{1/2} c \pi^{-1/2} t^{-1/2} \quad (3)$$

Where n is the total number of electron transfer, F is the Faraday's constant, A is the area of the electrode, D is the diffusion coefficient, c is the methanol concentration and t is time. The methanol oxidation is considered to be catalyzed by Ni-based catalysts in alkaline electrolytes through a four electron process as the following equation [32]:



The catalytic rate constant k_{cat} of the oxidation process can be calculated from the following equation [19]:

$$I_{\text{cat}}/I_{\text{L}} = \pi^{1/2}(k_{\text{cat}}ct)^{1/2} \quad (5)$$

Where I_{cat} and I_{L} represent the oxidation current in the presence and absence of methanol, respectively. And parameters k_{cat} , c and t indicate catalytic rate constant, methanol concentration and time, respectively. The catalytic rate constant k_{cat} can be obtained from the slope of $I_{\text{cat}}/I_{\text{L}}$ versus $t^{1/2}$ (Figure 8C). The value of k_{cat} is calculated to be $1.66 \times 10^6 \text{ cm}^3 \text{ mol}^{-1} \text{ s}^{-1}$.

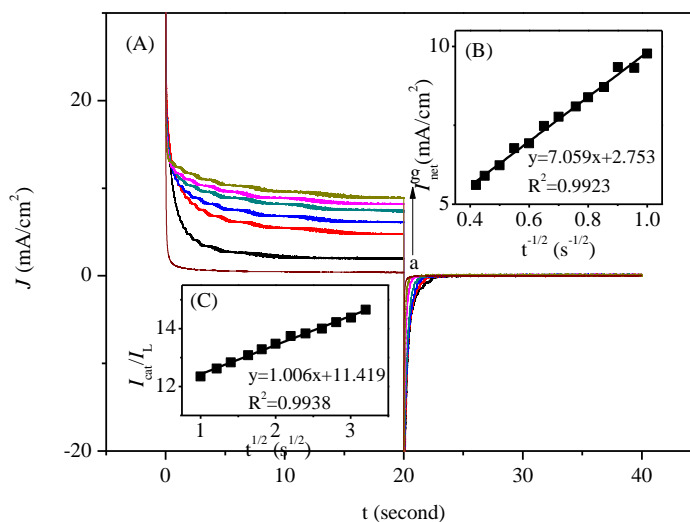


Figure 8. Chronoamperograms of Ni/Al₂O₃-5 in 0.1 M NaOH solution containing (a) 0 M, (b) 0.02 M, (c) 0.05 M, (d) 0.1 M, (e) 0.12 M, (f) 0.15 M, (g) 0.2 M methanol. Inset (B): Dependency of net current I_{net} on $t^{-1/2}$, derived from the data of chronoamperograms. Inset (C): Dependency of $I_{\text{cat}}/I_{\text{L}}$ on $t^{1/2}$, derived from the data of chronoamperograms.

4. CONCLUSION

In this work, ordered mesoporous Ni/Al₂O₃ catalysts were prepared by the solvent evaporation induced self-assembly (EISA) method. XRD, EDS mapping analyses, TEM and N₂ adsorption-desorption results indicate that Ni/Al₂O₃ catalysts obtain ordered mesoporous structure and high nickel dispersion. The methanol electrooxidation behavior was investigated by cyclic voltammetry and chronoamperometry. CVs results showed good electrocatalytic activity of Ni/Al₂O₃ for methanol oxidation in alkaline medium. This can be attributed to the ordered mesoporous structure and high nickel dispersion of Ni/Al₂O₃. The catalytic rate constant of methanol oxidation is calculated to be

$1.66 \times 10^6 \text{ cm}^3 \text{ mol}^{-1} \text{ s}^{-1}$ by chronoamperometric studies, and the methanol oxidation process is under methanol diffusion controlled.

ACKNOWLEDGEMENTS

This work is supported by the joint funds of the national natural science foundation of China–China Petroleum and Chemical Corporation (the state key program grant No.U1463209) and the national natural science foundation of China (grant No. 21371129; 21376157).

References

1. H. Liu, C. Song, L. Zhang, J. Zhang, H. Wang and D. P. Wilkinson, *J. Power Sources*, 155 (2006) 95.
2. R. Dillon, S. Srinivasan, A. S. Aricò and V. Antonucci, *J. Power Sources*, 127 (2004) 112.
3. M. Revenga–Parra, T. García, E. Lorenzo and F. Pariente, *Sensor. Actuat B: Chem.*, 130 (2008) 730.
4. J. M. Yang, S. A. Wang, C. L. Sun and M. D. Ger, *J. Power Sources*, 254 (2014) 298.
5. J. Wang, J. Xi, Y. Bai, Y. Shen, J. Sun, L. Chen, W. Zhu and X. Qiu, *J. Power Sources*, 164 (2007) 555.
6. J. H. Kim, H. K. Kim, K. T. Hwang and J. Y. Lee, *Int. J. Hydrogen Energy*, 35 (2010) 768.
7. A. V. Tripković, K. D. Popović, B. N. Grgur, B. Blizanac, P. N. Ross and N. M. Marković, *Electrochim. Acta.*, 47 (2002) 3707.
8. E. R. Choban, J. S. Spendelow, L. Gancs, A. Wieckowski and P. J. A. Kenis, *Electrochim. Acta.*, 50 (2005) 5390.
9. E. H. Yu and K. Scott, *J. Appl. Electrochem.*, 35 (2005) 91.
10. J. B. Raoof, R. Ojani and S. R. Hosseini, *J. Power Sources*, 196 (2011) 1855.
11. H. T. Zheng, Y. Li, S. Chen and P. K. Shen, *J. Power Sources*, 163 (2006) 371.
12. Z. Mojović, P. Banković, N. Jović–Jovičić, *Int. J. Hydrogen Energy*, 36 (2011) 13343.
13. A. Samadi–Maybodi, S. Ghasemi and H. Ghaffari–Rad, *J. Power Sources*, 303 (2016) 379.
14. Q. Yuan, A. X. Yin, C. Luo, L. D. Sun, Y. W. Zhang, W. T. Duan, H. C. Liu and C. H. Yan, *J. Am. Chem. Soc.*, 130 (2008) 3465.
15. F. Hahn, B. Beden, M. J. Croissant and C. Lamy, *Electrochim. Acta.*, 31 (1986) 335.
16. F. Hahn, D. Floner, B. Beden and C. Lamy, *Electrochim. Acta.*, 32 (1987) 1631.
17. Y. Hu, Y. V. Tolmachev and D. A. Scherson, *J. Electroanal. Chem.*, 468 (1999) 64.
18. Y. C. Weng, J. F. Rick and T. C. Chou, *Biosens. Bioelectron.*, 20 (2004) 41.
19. I. Danaee, M. Jafarian, F. Forouzandeh, F. Gobal and M. G. Mahjani, *Int. J. Hydrogen Energy*, 33 (2008) 4367.
20. B. Kaur, R. Srivastava and B. Satpati, *ACS Catalysis*, 6 (2016) 2654.
21. M. Asgari, M. G. Maragheh, R. Davarkhah, E. Lohrasbi, A. N. Golikand, *Electrochim. Acta.*, 59 (2012) 284.
22. A. Nozad Golikand, S. M. Golabi, M. Ghannadi Maragheh, L. Irannejad and M. Asgari, *J. Iran Chem. Soc.*, 4 (2007) 304.
23. J. B. Raoof, N. Azizi, R. Ojani, S. Ghodrati, M. Abrishamkar and F. Chekin, *Int. J. Hydrogen Energy*, 36 (2011) 13295.
24. R. Ojani, J. B. Raoof, S. Fathi and S. Alami–Valikchali, *J. Solid State Electrochem.*, 15 (2011) 1935.
25. S. N. Azizi, S. Ghasemi and E. Chiani, *Electrochim. Acta.*, 88 (2013) 463.
26. S. K. Hassaninejad–Darzi and M. Rahimnejad, *J. Iran Chem. Soc.*, 11 (2014) 1047.

27. A. A. El-Shafei, *J. Electroanal. Chem.*, 471 (1999) 89.
28. A. Ciszewski, G. Milczarek, B. Lewandowska and K. Krutowski, *Electroanal.*, 15 (2003) 518.
29. S. N. Azizi, S. Ghasemi and H. Yazdani-Sheldarrei, *Int. J. Hydrogen Energy*, 38 (2013) 12774.
30. W. Wang, R. Li, X. Hua and R. Zhang, *Electrochim. Acta.*, 163 (2015) 48.
31. I. Danaee, M. Jafarian, A. Mirzapoor, F. Gobal and M. G. Mahjani, *Electrochim. Acta.*, 55 (2010) 2093.
32. A. N. Golikand, S. Shahrokhian, M. Asgari, M. Ghannadi Maragheh, L. Irannejad and A. Khanchi, *J. Power Sources*, 144 (2005) 21.

© 2017 The Authors. Published by ESG (www.electrochemsci.org). This article is an open access article distributed under the terms and conditions of the Creative Commons Attribution license (<http://creativecommons.org/licenses/by/4.0/>).